Available online at www.sciencedirect.com
SCIENCE DIRECT®
Coordination Chemistry Reviews 249 (2005) 2567–2576
COORDINATION CHEMISTRY REVIEWS
www.elsevier.com/locate/ccr

Review

Magnetic exchange interactions in tetrabromocuprate compounds

Mark M. Turnbull [a,*], Christopher P. Landee [b], Brian M. Wells [b]

[a] *Carlson School of Chemistry and Biochemistry, Clark University, 950 Main St., Worcester, MA 01610, USA*
[b] *Department of Physics, Clark University, 950 Main St., Worcester, MA 01610, USA*

Received 30 September 2004; accepted 23 January 2005
Available online 21 February 2005

This manuscript is dedicated to the memory of Nicholas Rosov, an outstanding teacher and scholar who left us too soon.

Contents

Abstract

Magnetic and structural data for 28 compounds containing the tetrabromocuprate ion are presented. The parameters which affect the strength and sign of the magnetic superexchange interaction via non-bonding contacts between bromide ions are described and a system for describing the topology of the interaction between tetrahedra is proposed. Analysis of the data suggests that the primary factors affecting the magnetic exchange are the Br···Br distance, the Cu–Br···Br angle and the Cu–Br···Br–Cu dihedral angle.

Keywords: Tetrabromocuprate; Magnetic exchange; Copper compounds; Topology

* Corresponding author. Tel.: +1 50 879 37167; fax: +1 50 879 38861.
E-mail address: mturnbull@clarku.edu (M.M. Turnbull).

0010-8545/$ – see front matter © 2005 Elsevier B.V. All rights reserved.
doi:10.1016/j.ccr.2005.01.015

1. Introduction

1.1. Magnetic exchange via non-bonding halide–halide contacts

The propagation of and the possible mechanisms for magnetic exchange have been a major area of study for decades and numerous empirical and theoretical descriptions have been presented [1]. A variety of pathways are known to propagate the exchange, including single atoms or ions, such as halides, bridging between metal species [2]. Subsequently, it was discovered that magnetic exchange could propagate through non-bonding contacts between halide ions attached to different metal ions (this pathway, M–X···X–M, will be described as a double halide bridge). In their studies of $(H_3NCH_2CH_2NH_3)CuCl_4$, a compound consisting of sheets of square planar $CuCl_4^{2-}$ ions linked into square layers by Cu–Cl–Cu bridges, Drumheller and co-workers [3] made the observation that the antiferromagnetic exchange between the layers was approximately 60 times larger than the predicted value based upon the number of intervening atoms [4]. Subsequent work by the same group with a series of alkyldiammonium salts clearly showed that the effect was not unique to $(H_3NCH_2CH_2NH_3)CuCl_4$ and that the strength of the exchange was a function of the distance between the *halide ions*, rather than the distance between the metal ions [5]. Two additional critical points were reported in that work. The first was the observation that similar exchange occurred through a bromide–bromide bridge and that the exchange was significantly stronger, so that the compound $(H_3NCH_2CH_2NH_3)CuCl_2Br_2$ was best described as antiferromagnetic chains perpendicular to the layer structure, weakly linked by ferromagnetic Cu–Cl–Cu pathways [5]. The second was that the compound $[H_3N(CH_2)_4NH_3]CuCl_4$ did not appear to fit the trend observed for the other members of the class. One possible explanation for this was the exchange pathway, Cu–Cl···Cl–Cu, was not linear as it was in the other complexes, suggesting that the exchange interaction is dependant upon the geometry of the Cu–X···X–Cu pathway as well as the distance between the halide ions, as previously suggested by the work of van Kalkeren and co-workers [6]. Subsequent theoretical work by Block and Jansen [7] and later by Menon et al. [8] supported the idea of magnetic superexchange propagated through this double halide pathway. Further studies by Drumheller and co-workers [9,10] and Halvorson and Willett [11] on the structure and magnetic interactions in the $[H_3N(CH_2)_nNH_3)]CuBr_4$ family and theoretical work by Block and co-workers [12] verified that magnetic exchange interactions were propagated via the Br···Br bridge as well and that they were significantly stronger in all cases than their chloride counterparts. Subsequent work has shown that through-space X···X exchange is evident between pseudo-tetrahedral CuX_4^{2-} ions as well (see below).

The factors controlling the sign and strength of the magnetic exchange through the double halide bridge have not been delineated. An analysis of the relationship of geometric parameters to magnetic exchange in bridged copper(II) halides showed that virtually all of the potential variables had an effect on the magnitude and sign of J [13]. The magnetic interactions through Br···Br bridges are stronger than those for Cl···Cl bridges and those interactions are expected to have a greater dependence upon the geometric constraints of the system [13,14].

A wide variety of complexes have been synthesized which have the potential to exhibit magnetic superexchange through a double halide bridge. In the present work, we have limited our study to complexes with a $CuBr_4^{2-}$ ion where both the magnetic behavior and the crystal structure of the complex have been reported. The bromides show larger magnetic exchange, thus there is more reliable data available. Due to the large number of variables involved in the contacts between $CuBr_4^{2-}$ moieties, no quantitative magneto-structural correlations were anticipated, but trends should become clear from comparison of the compounds examined. We begin with definitions of the geometric variables, followed by presentation of a system for defining the topology of the interaction between the $CuBr_4^{2-}$ polyhedra.

1.2. Geometric variables

The factors that control the sign and strength of the magnetic exchange through the double halide bridge are not known at this time, but if we assume that it is dependant upon both the degree of delocalization of spin density from the Cu(II) ion to the halide and the orbital overlap between the two non-bonding halide ions, a number of variables become apparent. The structure of the $CuBr_4^{2-}$ ion itself will determine the degree of delocalization of spin density. This delocalization of spin density has been demonstrated by EPR and is substantial (∼50%) [15]. The Cu–Br bond length can be measured directly from X-ray data, but the bond angles become more cumbersome due to their greater number. $CuBr_4^{2-}$ can occur in tetrahedral or square-planar geometries. Idealized tetrahedra are not found in Cu(II) complexes due to the Jahn-Teller distortion and rigorously square-planar systems are rare, except in the perovskite layer compounds. The vast majority of $CuBr_4^{2-}$ complexes exhibit roughly D_{2d} symmetry and the degree of distortion from either tetrahedral or square-planar can be described via the *mean trans angle* (mta). For an idealized tetrahedron, the bond angles are all 109.5°. The Jahn-Teller distortion tends to flatten the tetrahedron, driving it toward a square-planar geometry, expanding two of the Br–Cu–Br angles. We define the two enlarged angles as the *trans*-angles and use the average of the two to define the distortion (mta). This is obviously a limited approximation and it becomes less suitable if the difference between the two *trans*-angles is large (that is, the distortion is not symmetrical).

The interactions between the ions have two components: one relating to the features of the tetrahedra that are in close contact (topological) and one relating to the geometry of each individual Cu–Br···Br–Cu interaction. The four parameters

d – The distance between the Br atoms

θ_1 – The angle Cu_1-Br_1….Br_2

θ_2 – The angle Cu_2-Br_2….Br_1

τ – The dihedral angle Cu_1–Br_1 ….Br_2–Cu_2

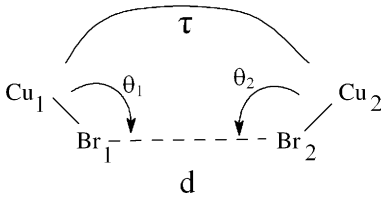

Fig. 1. Geometric parameters for describing the interaction between two $CuBr_4^{2-}$ ions.

necessary for describing each potential Cu_1–$Br_1\cdots Br_2$–Cu_2 interaction are given in Fig. 1.

1.3. Interaction topology

The proposed topological system is based upon the fundamental features of a tetrahedron: corners, edges and faces. Thus, the interactions are described in terms of which features of the two tetrahedra come into closest contact. The limit of the interaction (that is, which pieces are "in contact") is determined by measuring the closest contact between any two bromide ions (corners) and considering any distance within 10% of that distance as significant. The choice of 10% is arbitrary, but does have support based on experimental data where distance differences of 10% produce significant changes in the strength of magnetic interactions (see below). The interactions are organized by the interacting feature of the tetrahedron of the smallest dimensionality: corner (0), edge (1), or face (2).

A symbol is given, *n ij*(*d*), which designates the topology of the interaction (*i*,*j*), the number of such interactions (*n*) for a given tetrahedron and the shortest contact distance between the tetrahedra (*d*). The topologies are denoted c (corner), e (edge) and f (face). One symbol is required for each unique interaction of each tetrahedron in the asymmetric unit. The distance (*d*) is not required for purely topological descriptions, but will prove useful in initial analysis of the relationship between the types of interactions and the strength of the magnetic exchange. Consider the possible interactions using the lowest dimension of the interaction as the basis.

1.3.1. Corners

If one of the tetrahedra has only a corner involved in the interactions, the interaction falls in the corner class (Fig. 2). There are three limiting possibilities.

1.3.2. Edges

An interaction is classed as an edge interaction if the lowest dimensional contact between tetrahedra is an edge (Fig. 3). There are three possible edge–edge interactions depending on the relative distances between the ends of the two edges and depending on whether those edges are roughly parallel (Types 1 and 2) or roughly perpendicular (Type 3).

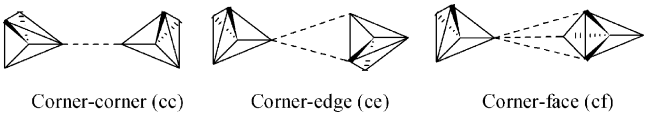

Fig. 2. Interactions types between tetrahedra involving a corner.

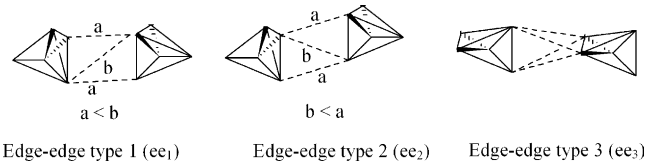

Fig. 3. Interactions between tetrahedra involving edges.

In Type 1 (ee_1), the defining feature of the edge–edge interaction is that the diagonal (*b*) of the parallelogram formed between the edges of the two tetrahedra is longer than a side (*a*). In Type 2 (ee_2), the shortest diagonal of the parallelogram (*b*) is shorter than a side (*a*). In Type 3, the edges are oriented nearly perpendicular, so that connection of the ends of the edges generates a (distorted) tetrahedron. Finally, the principle interaction could be between an edge of one tetrahedron and a face of the second (Fig. 4).

1.3.3. Faces

There are two possible topologies for the interaction between faces of two tetrahedra (Fig. 5). In one case, the figure formed by the closest connections of the corners of the two faces generates a trigonal prism (Type 1) while in the other case, the figure formed is a trigonal antiprism (Type 2).

These all represent limiting cases and real geometries are likely to be intermediate between these choices. In such cases, the choice of topology should be based upon the shortest contact distances between the X atoms.

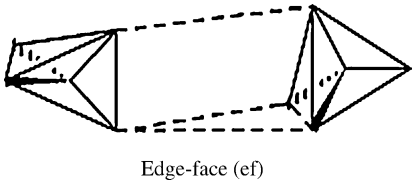

Fig. 4. Interaction between an edge and a face of tetrahedra.

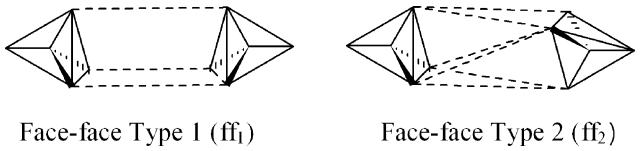

Fig. 5. Interactions between two faces of tetrahedra.

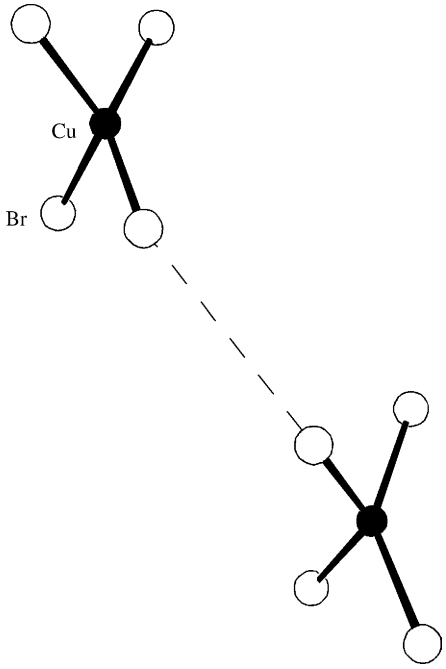

Fig. 6. Interaction within layers of bis(2-amino-5-chloropyridinium) tetrabromocuprate.

1.4. Examples

1.4.1. Bis(2-amino-5-chloropyridinium) tetrabromocuprate [16]: a square lattice

In this crystal ($C2/c$), each $CuBr_4^{2-}$ tetrahedron shows four identical interactions within a layer of the corner–corner type with a closest contact distance of 4.3 Å (Fig. 6). Therefore, the in-plane interactions are described as [4cc(4.3)]. The diagonal interaction within the plane (not shown) would be denoted [$2ee_1$(7.7)].

Between the planes, there are two edge–edge interactions for each $CuBr_4^{2-}$ tetrahedron, again identical by symmetry (Fig. 7). This is categorized as [$2ee_1$(4.8)], although in this particular case, the diagonal is more than 10% longer than the sides and thus is not categorized as an "interaction". There is also a diagonal interaction between the planes which is denoted [4cc(6.2)]. In examining the possible magnetic exchange interactions, only the [4cc(4.3)] and [$2ee_1$(4.8)] interactions were considered due to the very large distances in the other two possible interactions [16].

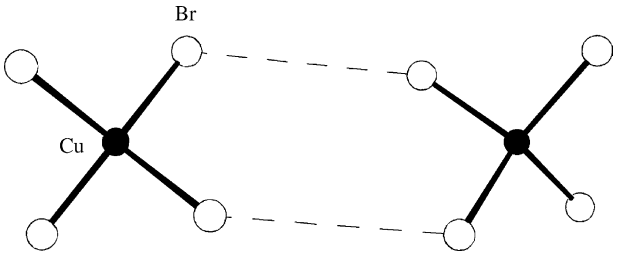

Fig. 7. The interlayer interaction in bis(2-amino-5-chloropyridinium) tetrabromocuprate.

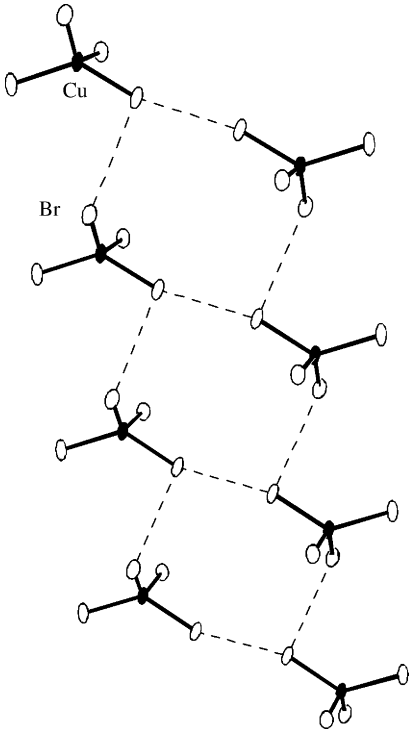

Fig. 8. Interactions in bis(2-amino-5-iodopyridinium) tetrabromocuprate dihydrate.

1.4.2. Bis(2-amino-5-iodopyridinium) tetrabromocuprate dihydrate [17]: a ladder

Only one $CuBr_4^{2-}$ tetrahedron occurs in the asymmetric unit, but in this case there are multiple interactions to be considered due to the lower symmetry (P-1) (Fig. 8). The rail interactions of the ladder are described as [2cc(4.2)]. The rung interaction is classed as [1cc(3.6)]. In addition, there may be a significant interaction across the short diagonal of the ladder [1ce(5.7)], but again the large distance makes it unlikely. The closest inter-ladder interaction is [1cc(5.5)].

1.4.3. Bis(2-amino-5-nitropyridinium) tetrabromocuprate hydrate [18]: a ladder

Again there is only one $CuBr_4^{2-}$ tetrahedron in the asymmetric unit, symmetry P-1 (Fig. 9). Here the rail interactions are [2cc(3.9)], while the rung interaction is [$1ee_2$(4.1)]. The rung diagonal is [$1ee_2$(4.7)] and could provide a measurable interaction. The closest interactions between ladders is [$1ee_1$(5.2)].

2. Data acquisition and analysis

A search of the literature was performed to identify compounds containing the $CuBr_4^{2-}$ moiety where both the crystal structure and magnetic exchange value had been determined [19]. From the crystal structure data, the geometric parameters for the major Br···Br non-bonding contacts were determined: Cu–Br bond length, Br···Br distance, Cu–Br···Br

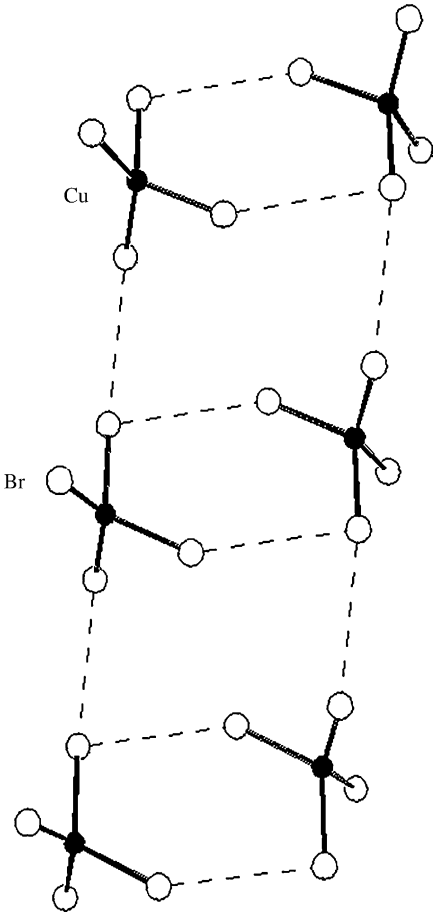

Fig. 9. Interactions in bis(2-amino-5-nitropyridinium) tetrabromocuprate hydrate.

angles, Cu–Br···Br–Cu torsion angles and the mean *trans*-angle for the $CuBr_4^{2-}$ ion. The major contacts were determined based upon the shortest Br···Br contacts in the lattice, including all contacts within 10% of the shortest. Additional contacts up to 5.0 Å are also listed in Table 1. In addition, the type of lattice formed by the short through-space Br···Br contacts was determined and the type of contact between the polyhedra identified (see Section 1.2). In some cases (see Table 1) the authors analyzed their data via the possibility of other superexchange pathways (hydrogen-bonding, π-stacking, etc.). In such cases, the lattice was reevaluated in terms of the bromide–bromide contacts and the value of *J* adjusted if necessary to provide an estimate of the exchange constant under the new lattice conditions. For example, a uniform chain will have a temperature at χ_{max} of 1.28 (J/k) whereas in a uniform square lattice, the temperature of χ_{max} occurs at 1.82 (J/k) [20]. Thus, given the exchange constant from a uniform chain fit to a data set (J_{1D}), the equivalent exchange constant for a two-dimensional system, $J_{2D} = (1.28/1.82)J_{1D}$. Such changes from the reported literature values are noted in Table 1. In total, 28 compounds were characterized and the results are given in the table. Compounds **14** [37] and **20** [32] from Table 1 were prepared according to the literature procedures and their temperature dependant magnetic susceptibilities determined in the range 1.8–325 K on a Quantum Design MPMS SQUID magnetometer. Corrections were made for diamagnetic contributions of the samples according to Pascal's constants and for temperature independent paramagnetism. X-Ray powder patterns were obtained on a Bruker AXS system and compared to published crystal data using Topas-2 [21].

3. Results

3.1. Antiferromagnetic interactions between pseudo-tetrahedral $CuBr_4^{2-}$ ions

Data were analyzed with respect to trends in the value of the exchange constant, *J*, relative to the various geometric parameters. Examination of the compounds with pseudo-tetrahedral geometry showed that the range of Cu–Br bond lengths was small (2.36–2.41 Å) and the range for square-planar complexes was even smaller (2.42–2.45 Å). No attempts were made to correlate these data with the exchange values. However, there is an obvious trend associated with the Br···Br non-bonding separation. Fig. 10 shows the relationship between the Br···Br distance and the exchange constant for the square-planar $CuBr_4^{2-}$ ions. The rapid decrease of $|2J|$ with increasing Br···Br separation is clear and has been previously noted to be exponential [11].

This family of compounds is particularly suitable for demonstrating the expected effect of distance on the exchange constant since all of the other geometric parameters remain virtually unchanged through the series.

The same general trend of decreasing $|2J|$ with increasing distance can also be seen in the interactions in the pseudo-tetrahedral complexes, but in this case there is great scatter in the data as a result of the wide variation in remaining variables (see Fig. 11). The trend is more obvious for interactions of the corner–corner type than for interactions of the edge–edge variety.

The wide scatter in the data clearly indicates that other parameters have a significant effect on the strength of the interactions. However, in compounds where large differences

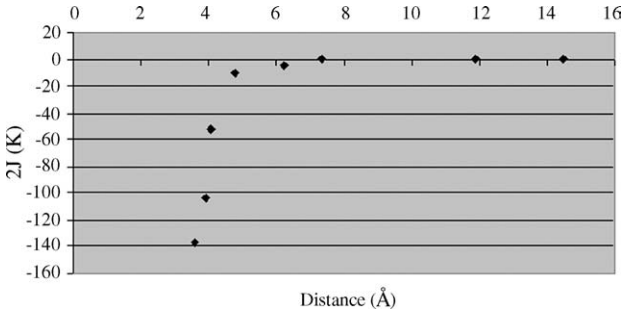

Fig. 10. Distance vs. 2*J* for square planar $CuBr_4$ complexes.

Table 1
Structural and magnetic data for the tetrabromocuprate complexes

	Formula	Cu geom.	Lattice	d Cu–Br (Å)	d Br···Br (Å)	θ Cu–Br···Br (°)	τ Cu–Br···Br–Cu (°)	mta (°)	Contact type	$2J/k$ (K)	Ref.
1	Catena-(ethylenediammonium) tetrabromocuprate										
	$C_2H_{10}N_2CuBr_4$	4 + 2	Fm square w/afm inter	2.45(×2)	3.60	157.7(×2)	180	180	2cc(3.60)	−136.8	[22,23]
2	Catena-(propylenediammonium) tetrabromocuprate										
	$C_3H_{12}N_2CuBr_4$	4 + 2	Fm square w/afm inter	2.45(×2)	4.06	155.8; 174.2	147.7	180	2cc(4.06)	−52	[22,24]
3	1,4-Butanediammonium tetrabromocuprate										
	$C_4H_{14}N_2CuBr_4$	4 + 2	Fm square w/afm inter	2.43(×2)	4.81	154.9(×2)	180	180	2cc(4.80)	−10	[24,25]
4	1,4-Pentanediammonium tetrabromocuprate										
	$C_5H_{16}N_2CuBr_4$	4 + 2	Fm square w/afm inter	2.44(×2)	6.23	149.2;167.2	165.5	180	2cc(6.23)	−4	[24,25]
5	3-Ammoniumpyridinium tetrabromocuprate										
	$C_5H_6N_2CuBr_4$	4 + 2	Fm square w/afm inter	2.44(×2)	3.90	162.9, 161.4	112	170.5	2cc(3.899)	−104	[26,27]
6	3-(Ammonium-methyl)pyridinium tetrabromocuprate										
	$C_6H_{10}N_2CuBr_4$	4 + 2 dist T_d	Fm layer w/afm inter	2.40 to 2.45	4.43	142–178	171–173	136, 180	2cc(4.43)	−11.6	[28]
7	bis(Beta-alaninium) tetrabromocuprate										
	$C_6H_{16}N_2O_4CuBr_4$	4 + 2	Fm square w/afm inter	2.43(×2)	7.34	170.7(×2)	104.75	180	2cc(7.34)	$J > 0$	[29]
8	bis(Morpholinium) tetrabromocuprate										
	$C_8H_{20}N_2O_2CuBr_4$	Dist. T_d	Dist. honeycomb	2.41; 2.36 2.37; 2.41	4.10/4.22 3.82	77.1, 139.3 140.151.5	20.2/180 53	134.6	1ee1(4.10) 2cc(3.82)	−8.8 −42.6	[30,31]
9	bis(Pyridinium) tetrabromocuprate										
	$C_{10}H_{12}N_2CuBr_4$	Dist. T_d	Square	2.36(×2) 2.38(×2)	4.36 4.71	147.0, 126.7 134.0, 134.0	−111.2 −54.4	131.3	4cc(4.36) 1cc(4.71)	−4.46[a]	[32]
10	bis(2-Amino-5-bromopyridinium) tetrabromocuprate;										
	$C_{10}H_{12}N_2Br_2CuBr_4$	Dist. T_d	Square	2.38, 2.39 2.38, 2.39	4.41 4.85	138.9, 136.7 120.5, 140.1	21.6 20.7	139	4cc(4.4) 2ee1(4.85)	−6.94	[33]
11	bis(2-Amino-5-chloropyridinium) tetrabromocuprate										
	$C_{10}H_{12}N_2Cl_2CuBr_4$	Dist. T_d	Square	2.38, 2.39 2.38, 2.39	4.3 4.83	138.9, 137.0 122.0, 138.1	21.9 −21.1	137.5	4cc(4.3) 2ee1(4.83)	−8.7 −8.6	[16,34]
12	bis(2-Aminopyridinium) tetrabromocuprate										
	$C_{10}H_{14}N_4CuBr_4$	Dist. T_d	Ladder, rung Rail	2.36(×2) 2.36, 2.39	4.35 4.13	97.8(×2) 144.2, 159.8	180 54.5	132.5	1cc(4.353) 2cc(4.127)	−6.8 −4.2	[30,35]
13	bis(2-Amino-5-nitropyridinium) tetrabromocuprate monohydrate										
	$C_{10}H_{14}N_6O_5CuBr_4$	Dist. T_d	Ladder, rung Rail Rung diag	2.41,2.44 2.35,2.44 2.35.2.41	4.07 3.93 4.58	148.6, 92.3 132.5, 146.5 111.8(×2)	7.6 3.6 180	130	1ee1(4.07) 2cc(3.93) 1ee2(4.68)	−20.4 −19.5	[18,36]
14	bis(4-Aminopyridinium) tetrabromocuprate monohydrate										
	$C_{10}H_{16}N_4OCuBr_4$	Dist. T_d	Square	2.37,2.39	4.55	140.5, 146.7	95.15	132.6	4cc(4.55)	∼−1[b]; 0.98[b]	This work [37]
15	bis(2-Amino-5-iodopyridinium) tetrabromocuprate dihydrate										
	$C_{10}H_{16}N_4I_2O_2CuBr_4$	Dist. T_d	Ladder, rung rail	2.38(×2) 2.38(×2)	3.58 4.23	151.9, 151.9 129.0, 95.0	180 98	132.6	1cc(3.565) 2cc(4.234)	−13 −1.15	[36,17]
16	bis(Cyclopentylammonium) tetrabromocuprate										
	$C_{10}H_{24}N_2$ $CuBr_4$	Dist. T_d	Ladder, rung Rail	2.36, 2.37 2.36, 2.36 2.36, 2.39 2.36, 2.40	4.41 4.52 3.88 3.89	105.3, 133.8 103.2, 132.1 148.8, 151.0 149.8, 151.1	62.5 63.4 64.3 55.9	130.1 132.3	1ee1(4.40) 1cc(3.88) 1cc(3.89)	−5.5 −11.6	[38]

17	bis(Piperidinium) tetrabromocuprate										
	$C_{10}H_{24}N_2CuBr_4$	Dist. T_d	Ladder, rung	2.37, 2.38	4.1	115.1, 133.7	47.3	130.8	1ee1(4.1)	−13.3	[39,40]
			Rail	2.38, 2.39	4.31	146.0, 153.5	53		2cc(4.31)	−3.8	
18	Catena-bis(p-chloroanilinium) tetrabromocuprate										
	$C_{12}H_{14}Cl_2N_2CuBr_4$	4 + 2	Fm square w/afm inter	2.42(×2)	11.89	155.7,161.4	170.9	180	2cc(11.89)	∼0.01	[41]
19	bis(2-Methylpyridinium) tetrabromocuprate										
	$C_{12}H_{16}N_2CuBr_4$	Dist. T_d	Unif. chain	2.38,2.39	4.74	126.1, 132.3	17.2	130.8	2ee1(4.74)	−2.44	[32]
		C2/c	Herringbone	2.38(×2)	4.98	116.0, 116.0	180		2cc(4.98)		
			Square	2.38,2.39	5.30	107.9,127.3	61.9		2ee1(5.30)		
20	bis(3-Methylpyridinium) tetrabromocuprate										
	$C_{12}H_{16}N_2CuBr_4$	Dist. T_d		2.38(×2)	4.06	82.0(×2)	180	135.5[c]	1ee2(4.06)	+2.96	[32]
					4.22	146.1, 78.5	6.5				
				2.38,2.39	4.45	104.5,133.6	111.8		2ce(4.45)		
						103.9,161.3	84.4				
				2.38(×2)	4.65	152.8,163.1	4.7		2cc(4.65)		
21	bis(4-Methylpyridinium) tetrabromocuprate										
	$C_{12}H_{16}N_2CuBr_4$	Dist. T_d	Alt. chain	2.39(×2)	4.55	86.2, 86.2	180	129.7	1ee2(4.55)	−1.16	[32]
				2.34,2.39	4.77	142.1, 82.5	9				
				2.42,2.43	5.04	110.3,126.2	3.5		1ee1(5.04)		
22	bis(2-Amino-3-methylpyridinium) tetrabromocuprate										
	$C_{12}H_{18}N_4CuBr_4$	Dist. T_d	Complex	2.36,2.37	4.15	102.8,130.2	72.7	131.6	2ce(4.15)	∼−4[d]	[42]
				2.36,2.39	4.25	99.7,170.9	80.2	140.2			
				2.37,2.39	4.13	122.6,151.4	117.6		1cc(4.13)		
				2.36,2.37	4.22	126.7,150.0	60.1		1cc(4.20)		
23	bis(2-Amino-5-methylpyridinium) tetrabromocuprate										
	$C_{12}H_{18}N_4CuBr_4$	Dist. T_d	Square	2.37,2.39	4.55	133.7, 143.8	16	137.2	4cc(4.55)	−6.6	[43,16]
				2.37,2.39	4.97	140.2, 119.4	19.8		2ee1(4.97)		
24	bis(3-Ethylpyridinium) tetrabromocuprate										
	$C_{14}H_{20}N_2CuBr_4$	Dist. T_d	Unif. chain	2.37,2.39	4.21	109.1, 151.4	3.8	130.1	2ee1(4.21)	−2.44	[44]
25	bis(4-Ethylpyridinium) tetrabromocuprate										
	$C_{14}H_{20}N_2CuBr_4$	Dist. T_d	Alt. chain	2.37(×2)	4.02	142.0, 142.0	180	137.4	1cc(4.02)	−4.32	[44]
				2.38(×2)	4.46	136.4, 136.4	180		1cc(4.46)	−3.456	
26	Catena-bis(2-phenylethylammonium) tetrabromocuprate										
	$C_{16}H_{24}N_2CuBr_4$	4 + 2	Fm layers w/Fm inter	2.45(×2)	14.7	160.2,165.5	170.4	180	4cc(14.7)	<1	[45,46]
27	bis(Methyl(phenylethyl)ammonium tetrabromocuprate										
	$C_{18}H_{28}N_2CuBr_4$	Dist. T_d	Unif. chain	2.36,2.40	4.13	79.9(×2)	180	142.1	2ee2(4.129)	−8.0	[47,30]
28	Catena-tetrakis(4-aminopyridinium) bis(dibromocuprate(I)) tetrabromocuprate										
	$C_{20}H_{28}N_8Cu_2Br_4CuBr_4$	Dist. T_d	Unif. chain	2.37(×2)	5.60	92.6	101.7	126.2	2ee3(5.60)	$\theta \sim -1$K	[48]

[a] Value recalculated base on different lattice interpretation. See Section 2.
[b] The authors report a weak ferromagnetic exchange. We find weak antiferromagnetic interactions.
[c] The two trans-angles are nearly identical suggesting an unusually uniform distortion of the $CuBr_4^{2-}$ ion.
[d] Nearly identical fits were obtained from either a uniform chain or 2D-square model.

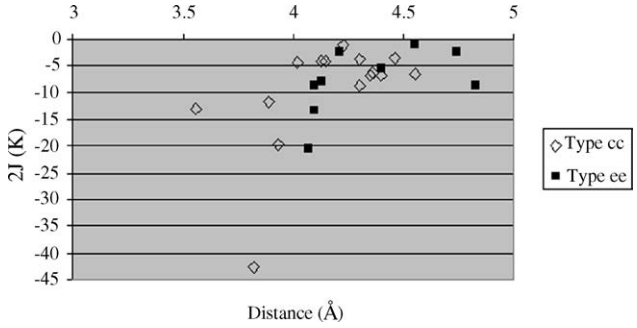

Fig. 11. Br···Br separation vs. 2*J*.

were seen in the Br–Br separation, only the shorter contacts were considered for further analysis.

Similarly, only general trends are obtained upon inspection of the effect of the Cu–Br···Br angle upon the value of the exchange constant. As was the case with distance, differences are seen in the behavior of the cc-interactions and the ee-interactions. Figs. 12 and 13 show the exchange constant plotted as a function of the sum of the two Cu–Br···Br angles for the cc- and ee-interactions, respectively. Although it is likely that different individual values for the two Cu–Br···Br angles which give the same total value could have very different interactions, there is insufficient data available to generate information based on individual angles, therefore only the sum of the two angles is used in the current discussion. For the cc-interactions, there is a slight trend toward increasing values of *J* with increasing angle. This suggests that as the Cu–Br···Br–Cu system approaches linearity, there is an increase in the magnetic exchange as might be assumed from

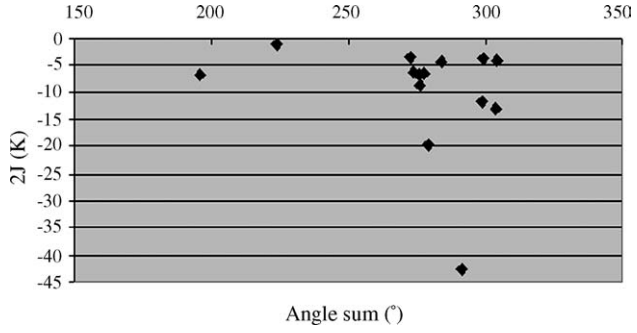

Fig. 12. Cu–Br···Br angle vs. 2*J* for cc interactions.

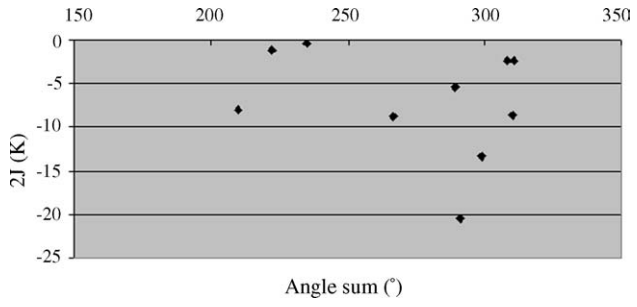

Fig. 13. Cu–Br···Br angle vs. 2*J* for ee interactions.

the expected increase in wave-function overlap. It is worth noting that for most of the square-planar systems, the sum of the Cu–Br···Br angles is between 310° and 330° and in general they show larger values of *J* than their tetrahedral counterpart at comparable Br···Br distances.

For edge–edge type contacts, the Cu–Br···Br angles are geometrically constrained from approaching 180°. The behavior is clearly different than that of the cc-compounds as can be seen in Fig. 13. The data are divided into two groups; those with angles in the 140–190° range have ee_2 and ee_3 interactions and those with angles in the 210–260° range are ee_1 type interactions. Each group shows a decrease in the exchange constant with increasing angle, the opposite of the trend observed for the cc-type complexes. For ee_1 interactions, assuming idealized tetrahedra and that the two interacting Br–Cu–Br pieces are coplanar, the sum of the two Cu–Br···Br angles is 250.5° and the majority of the data are clustered in that region. Deviations from the idealized angle indicate either distortion of the $CuBr_4^{2-}$ tetrahedron, lack of planarity of the Br–Cu–Br pieces, or both, reducing the symmetry of the system.

The same trend, decreasing *J* with increasing angles, is observed for ee_2 interactions, although there is no idealized angle sum since the Cu–Br···Br angles constitute a pair of alternate interior angles whose value will change with the distance between the $CuBr_4^{2-}$ ions. The limits will occur when the angle becomes so small that the interaction changes to an ee_1-type, or so large that the interaction become cc in nature. However, the small number of data available for this type of interaction suggests caution in any interpretation of these results.

No correlations are obvious when comparing the mean trans angle for the Cu(II) ion with the observed exchange constants (Fig. 14). The values of mta range from 126° to 142° with the only possible trend being that the variability of *J* seems to be smaller at higher angles, but this may be an artifact of the smaller number of data above 137°. A more likely correlation is seen in the relationship between the Cu–Br···Br–Cu torsion angle (τ) and the exchange constant (see Fig. 15). Again, there is a large spread in the data, but there is still a general correlation showing that the average values for *J* are larger for values of τ near 0° and near 180°. This

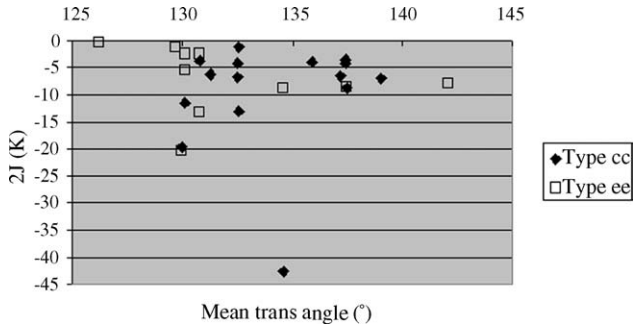

Fig. 14. Mean trans angle vs. 2*J*.

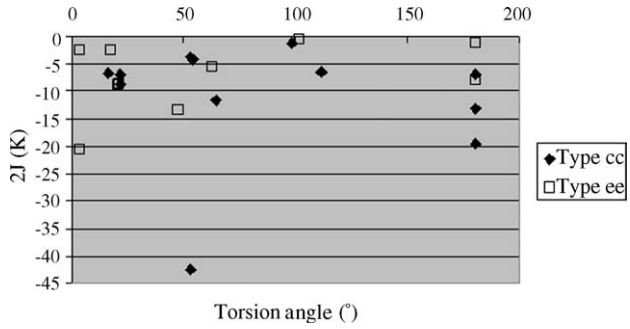

Fig. 15. –Cu–Br···Br–Cu torsion angle vs. 2*J*.

also makes sense in terms of orbital overlap which should be greatest at 0° (syn-periplanar) and at 180° (anti-periplanar).

3.2. Ferromagnetic interactions between pseudo-tetrahedral $CuBr_4^{2-}$ ions

Two compounds in Table 1 (Compounds **20** and **27**) deserve special comment as they are reported in the literature to exhibit ferromagnetic exchange, in complete contrast to all other reports of magnetism between $CuBr_4^{2-}$ tetrahedra via halide···halide contacts. We prepared bis(4-aminopyridinium) tetrabromocuprate monohydrate (Compound **14**, Table 1) according to the literature procedure [37] and confirmed its structure via IR and by comparison of its powder pattern to the published structure to ensure that the same phase had been produced. Magnetic susceptibility data were collected in an applied field of 1000 Oe from 1.8–325 K. The data show no indications of ferromagnetic interactions. Three separate preparations all indicated weak antiferromagnetic interactions with $\theta \sim -2$ K. The data provided equally good fits to models for either a uniform chain, or a square lattice with exchange constants of $2J < -1$. The anti-ferromagnetic behavior is in accord with expectations for halide···halide superexchange pathways.

In similar fashion, we prepared bis(3-methylpyridinium) tetrabromocuprate (Compound **20**, Table 1) and verified its structure with the literature [32]. Magnetic susceptibility data were again collected in an applied field of 1000 Oe from 1.8–325 K. To our surprise, our results matched the literature data and confirm the presence of ferromagnetic interactions in the sample. This is truly unusual as it appears to be a unique exception to the rule that halide···halide mediated exchange is anti-ferromagnetic. A more detailed examination of the structure suggested an explanation: the predominant superexchange pathway is not via the two-halide pathway, but rather via a single halide exchange, Cu–Br···Cu. The structure of the dimeric interaction in bis(3-methylpyridinium) tetrabromocuprate is shown in Fig. 16. The two-halide exchange interaction is of the ee_2 type [Br···Br = 4.06 Å]. However, in this case, the edges of the two distorted tetrahedra are offset sufficiently to allow for a symmetrical pair of short Br···Cu contacts between the $CuBr_4^{2-}$ ions [Cu–Br = 2.38 Å; Br···Cu = 4.414 Å; Cu–Br···Cu = 114°].

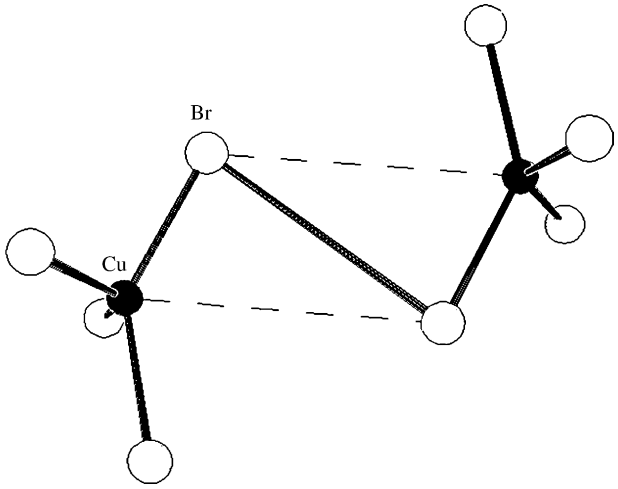

Fig. 16. Structure of the dimer interaction between adjacent $CuBr_4^{2-}$ ions in bis(3-methylpyridinium) tetrabromocuprate.

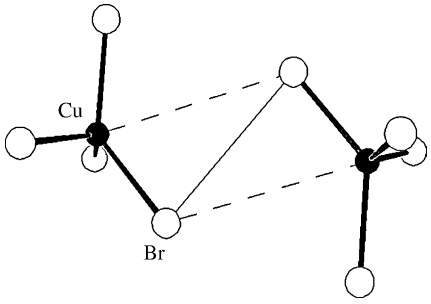

Fig. 17. Structure of the dimer interaction between adjacent $CuBr_4^{2-}$ ions in bis[methyl(phenylethyl)ammonium] tetrabromocuprate.

This type of single halide bridge has been previously reported to propagate ferromagnetic interactions and the geometry of this particular pair very closely resembles the interaction between the tetrahedral $CuBr_4^{2-}$ ions reported by Long et al. (Table 1, Compound **6**) [28]. The decrease in the magnitude of *J* is easily understood due to the increase in the Cu···Br distance (Cu···Br average of 4.2 Å in Compound **6**).

Examination of Table 1 shows a second compound with the same topological interaction, type ee_2, bis[methyl(phenylethyl)ammonium] tetrabromocuprate (Compound **27**, Table 1) [30]. Examination of the dimer structure (see Fig. 17) shows a nearly identical interaction (Cu–Br = 2.395 Å, Br···Cu = 4.40 Å, Cu–Br···Br = 112°; Br···Br = 4.13Å). However, the observed magnetic exchange in this complex is antiferromagnetic ($2J = -8$ K), so the topology itself cannot be the entire source of the explanation.

4. Conclusions

It is clear that the bromide···bromide superexchange pathway is complex and that multiple geometric factors influence the strength of the exchange. Based upon available data, it appears that the bromide···bromide distance and the

Cu–Br···Br angle play significant roles and there appears to be some correlation with the Cu–Br···Br-torsion angle. Other geometric factors are likely also to affect the exchange, but data available at present are too sparse to allow for reasonable speculation. In addition, results showing very weak exchange may contain significant influence from other superexchange pathways. Mechanisms including hydrogen bonding and π-stacking have been shown to support weak magnetic exchange and they may very well have a role in some of the compounds discussed. With one possible exception, all interactions between tetrahedral $CuBr_4^{2-}$ ions are antiferromagnetic. Calculations are in progress to attempt to resolve the question of ferromagnetic versus antiferromagnetic interactions and to determine the role of single halide versus double halide exchange in these complexes [49].

Acknowledgements

The MPMS SQUID was purchased with the assistance of the National Science Foundation – IMR-0314773. We are grateful for technical assistance to Mr. Lixin Li and Miss Qing Xu with the synthesis and magnetic measurements for bis(3-methylpyridinium) tetrabromocuprate and bis[methyl(phenylethyl)ammonium] tetrabromocuprate. We are also grateful for a gift from PolyCarbon Ind., Inc. toward the purchase of the X-ray diffractometer.

References

[1] (a) R.H. White, Quantum Theory of Magnetism, 2nd ed., Springer-Verlag, Berlin, 1983;
(b) R.L. Carlin, Magnetochemistry, Springer-Verlag, Berlin, 1986;
(c) O. Kahn, Molecular Magnetism, VCH Publishers, New York, 1993;
(d) L.J. Jongh (Ed.), Magnetic Properties of Layered Transition Metal Compounds, Kluwer Academic Publishers, Dordrecht, 1990.
[2] W.E. Marsh, E.J. Valente, D.J. Hodgson, Inorg. Chim. Acta 51 (1981) 49.
[3] L.O. Snively, P.L. Seifert, K. Emerson, J.E. Drumheller, Phys. Rev. B 20 (1979) 2101.
[4] L.J. deJongh, A.R. Miedema, Adv. Phys. 23 (1974) 1.
[5] L.O. Snively, G.F. Tuthill, J.E. Drumheller, Phys. Rev. B 24 (1981) 5349.
[6] G. van Kalkeren, W.W. Schmidt, R. Block, Physica 97 (1979) 315.
[7] R. Block, L. Jansen, Phys. Rev. B 26 (1982) 148.
[8] S. Menon, C. Balagopalakrishna, M.V. Rajasekharan, B.L. Ramakrishna, Inorg. Chem. 33 (1994) 950.
[9] G.V. Rubenacker, S. Waplak, S.L. Hutton, D.N. Haines, J.E. Drumheller, J. Appl. Phys. 57 (1985) 3341.
[10] L.O. Snively, D.N. Haines, K. Emerson, J.E. Drumheller, Phys. Rev. B 26 (1982) 5245.
[11] K. Halvorson, R.D. Willett, Acta Cryst. C 44 (1988) 2071.
[12] P. Straatman, R. Block, L. Jansen, Phys. Rev. B 29 (1984) 1415.
[13] R.D. Willett, in: R.D. Willett, D. Gatteschi, O. Kahn (Eds.), Magneto-Structural Correlations in Exchange Coupled Systems, Reidel, Boston, 1985, p. 389.
[14] P.J. Hay, S.C. Thibeault, R. Hoffmann, J. Am. Chem. Soc. 97 (1975) 4884.
[15] K. Chang, R.D. Willett, Inorg. Chim. Acta 4 (1970) 447.
[16] F.M. Woodward, A.S. Albrecht, C.M. Wynn, C.P. Landee, M.M. Turnbull, Phys. Rev. B 65 (2002) 144412.
[17] C.P. Landee, M.M. Turnbull, C. Galeriu, J. Giantsidis, F.M. Woodward, Phys. Rev. B: Rapid Commun. 63 (2001) 100402R.
[18] M.M. Turnbull, C. Galeriu, J. Giantsidis, C.P. Landee, Mol. Cryst. Liq. Cryst. 376 (2002) 469.
[19] (a) F.H. Allen, Acta Cryst. B 58 (2002) 380, Cambridge Structural Database;
(b) I.J. Bruno, J.C. Cole, P.R. Edgington, M. Kessler, C.F. Macrea, P. McCabe, J. Pearson, R. Taylor, Acta Cryst. B 58 (2002) 389, ConQuest.
[20] (a) J.C. Bonner, M.E. Fisher, Phys. Rev. 135 (1964) 640;
(b) J.-K. Kim, M. Troyer, PRL 80 (1998) 2705.
[21] Topas 2.1, Bruker AXS, 2000.
[22] K. Halvorson, R.D. Willett, Acta Cryst. C 44 (1988) 2071.
[23] G.V. Rubenacker, S. Waplak, S.L. Hutton, D.N. Haines, J.E. Drumheller, J. Appl. Phys. 57 (1985) 3341.
[24] L.O. Snively, D.N. Haines, K. Emerson, J.E. Drumheller, Phys. Rev. B 26 (1982) 5245.
[25] J.K. Garland, K. Emerson, M.R. Pressprich, Acta Cryst. C 46 (1990) 1603.
[26] N. Sivron, T.E. Grigereit, J.E. Drumheller, K. Emerson, R.D. Willett, J. Appl. Phys. 75 (1994) 5952.
[27] R.D. Willett, H. Place, M. Middleton, J. Am. Chem. Soc. 110 (1988) 8639.
[28] G.S. Long, M. Wei, R.D. Willett, Inorg. Chem. 36 (1997) 3102.
[29] R.D. Willett, R.J. Wong, M. Numata, Inorg. Chem. 22 (1983) 3189.
[30] P. Zhou, J.E. Drumheller, G.V. Rubenacker, K. Halvorson, R.D. Willett, J. Appl. Phys. 69 (1991) 5804.
[31] Recent reinterpretation of the data presented in reference 29 by the authors suggests that the original assignments of J values may have been reversed. The assignments in this paper have been adjusted accordingly. Additional detailed studies are in progress. R.D. Willett and R.T. Butcher, private communication.
[32] A. Luque, J. Sertucha, O. Castillo, P. Román, N. J. Chem. 25 (2001) 1208.
[33] F.M. Woodward, C.P. Landee, J. Giantsidis, M.M. Turnbull, C. Richardson, Inorg. Chim. Acta 324 (2001) 324.
[34] T. Matsumoto, Y. Miyazaki, A.S. Albrecht, C.P. Landee, M.M. Turnbull, M. Sorai, J. Phys. Chem. B 104 (2000) 9993.
[35] A. Luque, J. Sertucha, L. Lezama, T. Rojo, P. Román, J. Chem. Soc., Dalton Trans. (1997) 847.
[36] Calin Galeriu, M.A. Thesis, Synthesis and Magnetic Properties of Molecular-Based Spin-Ladder Systems, Clark University, 2001.
[37] P. Roman, J. Sertucha, A. Luque, L. Lezama, T. Rojo, Polyhedron 15 (1996) 1253.
[38] R.D. Willett, C. Galeriu, C.P. Landee, M.M. Turnbull, B. Twamley, Inorg. Chem. 43 (2004) 3804.
[39] B.R. Patyel, B.L. Scott, R.D. Willett, Phys. Rev. B 41 (1990) 1657.
[40] B.C. Watson, V.N. Kotov, M.W. Meisel, D.W. Hall, G.E. Granroth, W.T. Montfrooij, S.E. Nagler, D.A. Jensen, R. Backov, M.A. Petruska, G.E. Fanucci, D.R. Talham, Phys. Rev. Lett. 86 (2001) 5168.
[41] T. Sekine, T. Okuno, K. Awaga, Inorg. Chem. 37 (1998) 2129.
[42] T.J. Coffey, C.P. Landee, W.T. Robinson, M.M. Turnbull, M. Winn, F.M. Woodward, Inorg. Chim. Acta 303 (2000) 54.
[43] H. Place, Helen, R.D. Willett, Acta Crystallogr. C 43 (1987) 1050.
[44] A. Luque, J. Sertucha, O. Castillo, P. Román, Polyhedron 21 (2002) 19.
[45] P. Zhou, J.E. Drumheller, B. Patyal, R.D. Willett, Phys. Rev. B 45 (1992) 12365.
[46] R.D. Willett, Acta Crystallogr. C 46 (1990) 565.
[47] H. Place, R.D. Willett, Acta Crystallogr. C 44 (1988) 34.
[48] J. Sertucha, A. Luque, F. Lloret, P. Román, Polyhedron 17 (1998) 3875.
[49] F. Mota, J.J. Novoa, J. Ribas, private communication.